Available online at www.sciencedirect.com
SCIENCE DIRECT
Journal of Colloid and Interface Science 279 (2004) 175–185
JOURNAL OF Colloid and Interface Science
www.elsevier.com/locate/jcis

Using the Surface Evolver to model droplet formation processes in membrane emulsification

Marilyn Rayner *, Gun Trägårdh, Christian Trägårdh, Petr Dejmek

Lund University, Department of Food Technology, Engineering, and Nutrition, P.O. Box 124, 221 00 Lund, Sweden

Received 23 January 2004; accepted 23 June 2004

Available online 24 July 2004

Abstract

A model was developed to describe the droplet formation mechanism in membrane emulsification from the point of view of Gibbs free energy with the help of the Surface Evolver, which is an interactive finite element program for the study of interfaces shaped by surface tension. A program to test the model was written and run which allows the user to track the droplet shape as it grows, to identify the point of instability due to free energy, and thus predict droplet size. The inputs of the program are pore geometry, oil–aqueous phase interfacial tension, and contact angle. The model reasonably predicted droplet sizes for oblong-shaped pores under quiescent conditions where the force balance approach is not applicable. The model was validated against experimental conditions from the literature where the average error of the predictions compared to the mean droplet sizes was 8%.

Keywords: Membrane emulsification; Surface Evolver; Gibbs free energy; Modelling; Droplet formation

1. Introduction

Over the past decade there has been an increasing interest in a novel technique for making emulsions known as membrane emulsification. This process makes use of microporous membrane where continuous phase flows tangentially to the membrane surface and the dispersed phase is pressed through the membrane. Droplets of dispersed phase form at the openings of membrane pores and are continuously swept away by the flowing continuous phase (Fig. 1).

The key feature of the membrane emulsification process which sets it apart from conventional emulsification technologies is that the size distribution of the resulting droplets is primarily governed by the choice of membrane rather than the development of turbulent or extensional droplet breakup [1]. The main advantages of membrane emulsification include: the possibility to produce droplets of a defined size with a narrow size distribution, low shear stress, the potential for lower energy consumption, and simplicity of design [2].

There are quite a number of interesting applications of this process. As the size of the droplets can be designed, the resulting emulsion can be used as a controlled release system. Both oil-in-water and water-in-oil emulsions are possible (depending on the hydrophilic or hydrophobic nature of the membrane), as is the ability to form double emulsions. Food applications have included light margarine type spreads, mothers' milk replacements and the microencapsulation of flavors [3]. Due to the low shear stresses and mild processing conditions, shear sensitive materials could be incorporated. Membrane emulsification has also been used to produce uniform silica hydrogel beads, and polymer microspheres used in HPLC applications [4].

A close relative to membrane emulsification is microchannel emulsification which operates on the same principle of extruding the dispersed phase into the continuous phase, but differs with respect to the membrane. As the name implies, microchannel emulsification uses a microfabricated channel array on a silicon plate. A series of geometrically

* Corresponding author. Fax: +46-46-2224622.
E-mail address: marilyn.rayner@livstek.lth.se (M. Rayner).

0021-9797/$ – see front matter
doi:10.1016/j.jcis.2004.06.068

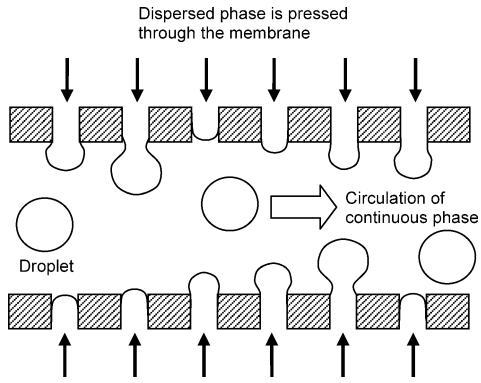

Fig. 1. Schematic illustration of the principle of membrane emulsification.

defined grooves in the silicon enclose three sides of each channel and a top-plate closes the fourth, creating a rectangular capillary through which the dispersed phase is pressed. These plates can be stacked to create a module to increase production output. To study the process in detail, a glass top-plate is used in a model setup which allows viewing the drops as they form using a microscope, yielding significant insight into the droplet formation process [5–8].

These two methods of making emulsions droplet by droplet have different practical aspects, but are governed, to a certain extent, by the same physical mechanisms. The final size of emulsion droplets is determined by the process parameters including: pore size or channel geometry, cross-flow velocity, dispersed phase flux, viscosity, and interfacial tension. The effects of these process parameters have been reported in the literature; however, the underlying physical mechanisms of droplet formation still require further examination, which is the basis of this work.

2. How drops detach

The size of drops when they detach from the membrane or microchannel depends on the above mentioned process parameters which have been evaluated by associating them to forces which act on the system [1,9]. The main forces identified in the literature are described below and illustrated in Fig. 2. The interfacial tension force, $F\gamma$, represents the effects of dispersed phase adhesion around the edge of the pore opening and is the key retaining force during droplet formation. The static pressure difference force, F_{sp}, is due to the pressure difference between the dispersed phase and the continuous phase at the membrane surface. The viscous drag force, F_D, is created by the continuous phase flowing past the droplet parallel to the membrane surface. The dynamic lift force, F_L, results from the asymmetric velocity profile of the continuous phase near the droplet. The buoyancy force, F_B, is due to the density difference between the phases. The inertial force, F_I, is associated with a mass of the fluid flowing out from the opening of the pore.

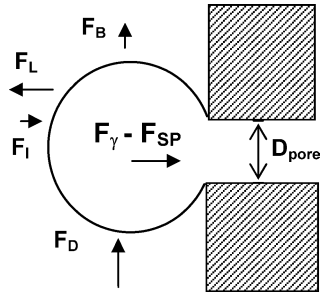

Fig. 2. Forces acting on a droplet.

The relative magnitude of these forces change as the droplet increases in size and has been plotted in the literature [1,9]. It has been shown that for micrometer scale droplets the inertia and buoyancy forces are approximately 9 and 6 orders of magnitude smaller respectively than the drag and interfacial tension forces (plotted in Fig. 3) and therefore can be neglected in the force balance type models. According to the current dogma, the point at which the droplet detaches after reaching a certain volume occurs when the sum of these forces acting on it equals zero.

How well these force balance models fit the data is hard to decipher from the literature. Peng and Williams [1] give an example of their plotted model with data from droplets forming from a large (45 μm) capillary under low wall shear stress. Schröder et al. [9] and Wang et al. [10] use a more elaborate force balance model but do not fit their experimental data against it. Rayner and Trägårdh [11] plotted predicted droplet size with experimental values. The model did follow the overall trend in the data, but diverges dramatically with different experimental conditions and gives at best an order of magnitude estimation at lower wall shear stresses. This leads one to imagine that the droplet formation story is more complicated than first anticipated, and subsequently provided the motivation for further investigations.

As discussed above, not all forces are significant on the microscopic scale. Sugiura et al. [6] considered droplet formation from a microchannel into a quiescent continuous phase through evaluating the dimensionless groups relevant to droplet formation, these being the Reynolds number (*Re*),

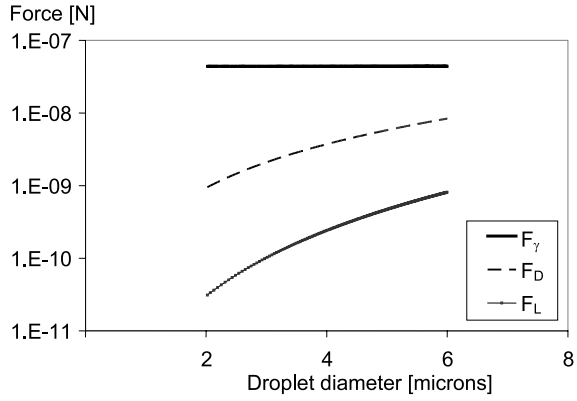

Fig. 3. Estimation of the forces acting on a droplet. Conditions: 29 Pa wall shear stress, 2 μm pore diam., interfacial tension 7 mN m^{-1}.

the Bond number (*Bo*), the Weber number (*We*) and the Capillary number (*Ca*). The relative magnitudes of these forces are given below for a typical membrane emulsification setup using a 1×10^{-6} m pore diameter, an interfacial tension of 5×10^{-3} N m^{-1} and a dispersed phase velocity of 1×10^{-3} m s^{-1}, oil density 8×10^{2} kg m^{-3}, and viscosity 5×10^{-2} Pa s:

$$Re = \frac{\text{inertial force}}{\text{viscous force}} = \frac{\rho D U}{\mu} = 2 \times 10^{-5}, \quad (1)$$

$$Bo = \frac{\text{gravitational force}}{\text{interfacial tension force}} = \frac{\Delta \rho g D^2}{\gamma} = 4 \times 10^{-7}, \quad (2)$$

$$We = \frac{\text{inertial force}}{\text{interfacial tension force}} = \frac{\rho D U^2}{\gamma} = 2 \times 10^{-7}, \quad (3)$$

$$Ca = \frac{\text{viscous force}}{\text{interfacial tension force}} = \frac{\mu U}{\gamma} = 1 \times 10^{-2}. \quad (4)$$

This simple calculation gives insight into the relative importance of the forces. From the numbers above, one can deduce that the interfacial tension force dominates this process.

Sugiura et al. [6] used the Capillary number to describe the flow formation in their microchannel, but more importantly presented a mechanism for interfacial tension driven droplet formation. This mechanism termed "spontaneous transformation based" droplet formation is described by considering the free energy of the system. In their setup the droplet was deformed by the rectangular geometry of the microchannel causing it to have a disc-like shape, which is unstable from the view point of free energy, ΔG, since it has a much greater interfacial area than a sphere of equivalent volume. The ability of a droplet to spontaneously form was calculated from the reduction in total interfacial area from before, A_1, and after, A_2, the droplet forms through estimating the interfacial areas from video images obtained using the setup described in [5]:

$$\Delta G = \gamma (A_2 - A_1). \quad (5)$$

They found that the geometry of the microchannel played a critical role in spontaneous transformation based (STB) droplet formation since it is essential that the droplet be deformed from its spherical, lowest energy shape. This type droplet deformation does not solely take place in microchannel emulsification, but is also observed in SPG (Shirasu porous glass) membrane emulsification [12] and in arrays of straight through holes in silicon plates [13–15]. This STB droplet formation mechanism could explain how droplets can be successfully formed without any cross-flow in the continuous phase [12] and what causes droplets to break off even when the force balance model predicts otherwise.

3. Objectives

The objectives of this present work were to quantify the process of droplet formation in terms of interfacial energies, to model the droplet shape as it grows, and to identify the point of instability due to free energy, and thus the beginning of the droplet detachment process. This modelling work was undertaken with the help of the software program Surface Evolver and the results are compared against experimental values found in the literature. This model uses only physical and geometric variables to describe the process and thus does not need to rely on a curve fitting exercise or the addition of empirical constants.

4. Method

4.1. Description of the Surface Evolver

The Surface Evolver is public domain finite element package [16], which was developed by Ken Brakke as part of an American National Science Foundation funded geometry supercomputing project. It is an interactive program for the study of surfaces shaped by surface tension and other energies, subject to various constraints. The user defines an initial surface in a data file. The program then evolves the surface toward minimal energy by a gradient descent method. The numerical algorithm based on Lagrange's principle of virtual works, proposing that a mechanical system in a state of equilibrium leads to a minimum in the system's total energy [16]. It is generally used for solving problems involving the minimization of surfaces [17–19] but has also seen more practical applications in the design of solder joints for microchips [20], prediction the wetting of fibers, [21] and the controlled production of liquid pillars used for pharmaceutical drug screening [22].

The Surface Evolver uses a triangular tessellation to represent surfaces, which can be progressively refined to achieve the desired level of accuracy. The Surface Evolver parameterizes surfaces in terms of its vertex coordinates for a particular triangulation and then modifies a given initial interface shape taking into account the requirements of the Gauss–Laplace equation. The shape of the droplet under a certain set of constraints is found by iteratively moving vertices using the Newton–Raphson method and will quickly converge the surface's energy to a local minimum [23]. The graph of the energy function could be imagined as a landscape of hills, valleys, and mountain passes. The gradient of the energy function, **G** can subsequently be thought of as the steepest up hill direction [24]. Each iteration step in the Evolver minimizes the energy by moving in the downhill direction, the negative gradient direction, until reaching a local minimum.

The code automatically takes into account the contributions of the interface to the system's energy, whereas the shape of the boundaries and the wetting energies arising there have to be added by the user by providing appropriate integration coefficients along the contact lines [17].

4.2. How the Surface Evolver detects surface instabilities

Surface Evolver provides a means to study droplet energies and surface areas to further our understanding of spontaneous transformation based formation processes. In this work we study the surfaces of drops which are both near a local minima and a point of instability by using eigenvector analysis. In this case eigenvectors represent a particular mode of surface perturbation. The energy cost of such a perturbation corresponds to the magnitude of their corresponding eigenvalues. This small movement creates a force in line with the perturbation direction. If the eigenvalue is positive, the force will act to restore the surface to its nearby equilibrium (stable perturbation) but if the eigenvalue is negative (similarly $-\Delta G$) the force will cause the perturbation to grow (unstable perturbation). By following the sign of the lowest eigenvalue, instability in a droplet is detected, and thus the point at which a droplet will spontaneously detach for a given set of parameters is found. For a more detailed description refer to the Surface Evolver tutorial on Hessian, eigenvalues, eigenvectors and stability techniques [24].

4.3. Gibbs free energy

Sugiura et al. (2001) used the change in Gibbs free energy (Eq. (5)) to show that droplet formation will occur spontaneously due to the nonminimized surface area of the droplet. It is important to bear in mind that Gibbs free energy is a thermodynamic function which is defined by

$$G \equiv H - TS = E + PV - TS, \tag{6}$$

where H is enthalpy, T is temperature, S is entropy, P is pressure, E is energy, and V is volume. The change in Gibbs free energy as a system undergoes a thermodynamical change is

$$dG = dE + P\,dV + V\,dP - T\,dS - S\,dT. \tag{7}$$

Recall that, the first law of thermodynamics states that a system may exchange energy with the surroundings strictly through heat flow or work, and the second law of thermodynamics governs how much internal energy can be converted to mechanical energy. In this two phase system the liquids can be considered incompressible and that the system is closed and isothermal (no heat flow); thus the free energy is equal to the work received by the system. Under these circumstances, the changes in Gibbs free energy ΔG and changes in Helmholtz free energy, df, are equal [25]:

$$dG = df = dE_{\text{mech}} = -dW. \tag{8}$$

The above work term, dW, is related to the surface by the fact that in order to produce an infinitesimal increase in the surface area, A, keeping the temperature and volume of the whole system constant, an infinitesimal amount of reversible work is required:

$$\delta W = -\gamma\,dA \tag{9}$$

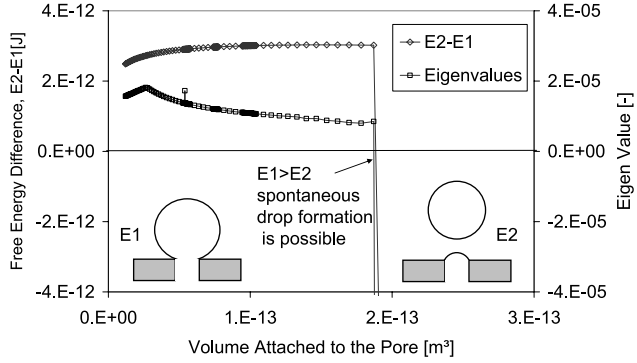

Fig. 4. Stability investigation to compare occurrence of negative free energy change and negative eigenvalues.

(note that δ indicates that this work is not a total differential).

We get the surface energy, E_{surf}, by adding up all the infinitesimal area increases:

$$E_{\text{surf}} = \int \gamma\,dA = \gamma A. \tag{10}$$

In the case of the droplet, we compare the difference in the change of free energy between before and after droplet detachment (Eq. (5)); but what is the volume of this droplet?

The maximum stable droplet volume can be found by charting the occurrence of negative eigenvalues from the Surface Evolver simulation as well as considering the change in free energy of the system. If one compares the free energy of the attached droplet (total energy found by the Surface Evolver, $E1$ in Fig. 4) to the energy of a droplet of equal volume plus the energy of the pore opening ($E2$ in Fig. 4), one can find the maximum stable volume, i.e., the volume just before a spontaneous transformation based droplet formation would take place. The left axis of Fig. 4 shows the free energy difference, i.e., $E1 - E2$. When the volume increases to the point that the $E1$ shape becomes unstable it can spontaneously change to $E2$ because the free energy difference between these two configurations is negative.

The Surface Evolver also finds the maximum stable droplet volume through eigenvector analysis as described above in Section 4.2. In Fig. 4 the occurrence of instability is shown from both a free energy difference perspective as well as using the lowest eigenvalue from the Surface Evolver calculation directly. Fig. 4 demonstrates that the occurrence of negative eigenvalues directly corresponds to the point at which the free energy difference becomes negative (spontaneous droplet formation). Thus the instability detected in the droplet by the Surface Evolver is confirmed. The droplet volume just before instability is taken to be the maximum stable volume (MSV) and yields an estimation of the largest droplet which should form. However, it is well known that a droplet is not popped clean off—there is a certain volume remaining at the pore that is a section of an ellipsoid (or sphere if the pore happens to be round) that includes some of this maximum stable volume. The question is: How much?

4.4. Pressure Pinch Constraint

Once the maximum stable volume is found, the amount which breaks away to form the droplet needs to be determined. Previously, others have used the Harkins–Brown correction factor [26] to describe the amount remaining at a capillary opening after droplet detachment [27–29]. This factor uses an empirical relation including the capillary diameter and volume of the detached droplet. However, this correction factor is based on drops forming from capillaries which are large enough that both gravity and inertia are included in the detachment model.

Here we propose an alternative break off description, called the "Pressure Pinch Constraint," based on the division of the surface into two volumes, a droplet and a segment of ellipsoid which remains attached to the pore mouth. The relative size of these two volumes is such that the resulting radii of curvature will maintain an equal Laplace pressure across the surface of both volumes. Another way to consider this is to imagine a long skinny balloon that is being pinched together somewhere along its length. No matter where one pinches it, the pressure must be the same in both segments. By using this Pressure Pinch Constraint we can calculate the allowable droplet volume that will have a Laplace pressure, P_{Laplace}, equal to that of the remaining segment attached to the pore. This is calculated directly from the total energy, area, and volume outputs from the Surface Evolver simulation using the Laplace equation [30]

$$P_{\text{drop}} - P_{\text{out}} = P_{\text{Laplace}} = \gamma \frac{dA}{dV}. \tag{11}$$

Note for a spherical droplet,

$$A = 4\pi R^2 \quad \text{and} \quad \frac{dA}{dR} = 8\pi R, \tag{12}$$

$$V = \frac{4}{3}\pi R^3 \quad \text{and} \quad \frac{dV}{dR} = 4\pi R^2, \tag{13}$$

and using the chain rule

$$\frac{dA}{dR}\frac{dR}{dV} = \frac{dA}{dV} = \frac{2}{R}, \tag{14}$$

yielding the commonly used (and in some cases misused) equation

$$P_{\text{Laplace}} = \frac{2\gamma}{R}. \tag{15}$$

The volume of the droplet that breaks off is V_{break} and is equal to the largest stable volume V_{final} minus the remaining attached volume, V_{attached}. The energy, E_{total}, and the volumes for all stable surfaces up to the instability point as the droplet grows are logged by the Surface Evolver. Using this information, Eqs. (8) and (10), and the Pressure Pinch Constraint we can solve for the radius of the detached droplet (Fig. 5). As the radius of the detaching droplet increases (x-axis in Fig. 5) the Laplace pressure of that droplet decreases, however the larger the detaching droplet the smaller the remaining piece is, and thus the pressure of the corresponding attached surface increases. From the above argument of the Pressure Pinch Constraint we know that these two pressures must be equal and thus we find the radius of the detaching droplet at the intersection of the pressure curves of the two surfaces, P_{break} and P_{attached}:

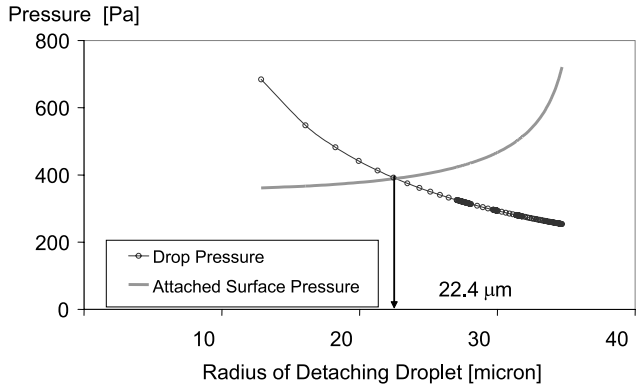

Fig. 5. Plot showing the size of the breakoff droplet using the pressure pinch constraint.

$$V_{\text{break}} = V_{\text{final}} - V_{\text{attached}}, \tag{16}$$

$$R_{\text{break}} = \sqrt[3]{\left(\frac{3}{4\pi}V_{\text{break}}\right)}, \tag{17}$$

$$P_{\text{break}} = \frac{2\gamma}{R_{\text{break}}} = P_{\text{attached}} = \frac{E_{\text{Laplace}}}{V_{\text{attached}}}, \quad \text{where } E_{\text{Laplace}} = E_{\text{total}} - E_{\text{pore}}. \tag{18}$$

In the case of a droplet forming from a pore, the pore itself also plays a role in determining the final curvature of the surface. E_{pore} is the energy contribution from the pore itself, i.e., at infinite curvature, and thus is subtracted.

4.5. Development of the droplet formation model

The model is defined as an initial surface in a data-file which is the input the Surface Evolver. The data file contains the geometric definition of the surface as vertices (points), edges (vectors), facets (triangles), and bodies (groups of oriented facets), as well as, constraints, methods and boundary conditions to calculate the various energies, and user defined macros which, among other things, help to display the surface, repeat commands, and pipe formatted output data to files.

The assumptions used in this model include:

(1) constant interfacial tension;
(2) no inertial, gravitational, or kinetic energy;
(3) drops are forming into a quiescent water phase.

The droplet formation model begins with an unrefined geometry. In this case the droplet is forming from an elliptical pore with a major axis $Rc1$ and minor axis $Rc2$ laying in the $x_3 = 0$ plane. This yields the geometric constraints which define the membrane, i.e., that the droplet is inside the pore

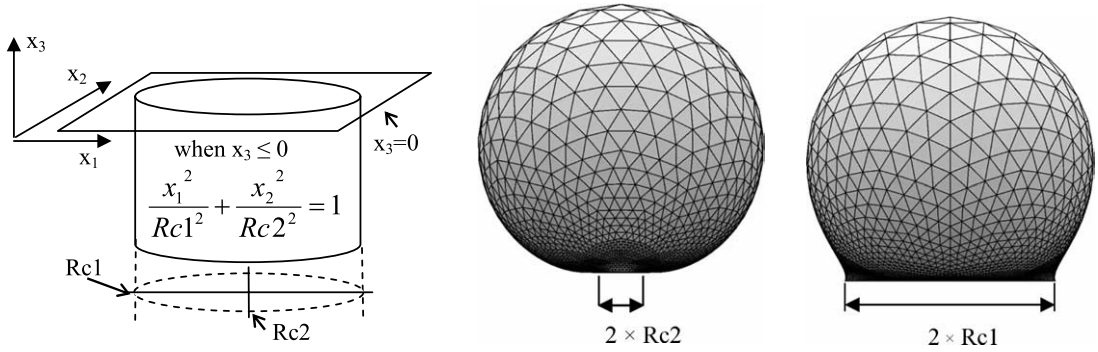

(a) (b) (c)

Fig. 6. (a) Pore boundary conditions. (b) Front view, where *Rc*2 is minor axis. (c) Side view, where *Rc*1 is major axis, of a refined droplet during simulation.

defined by the equation of an ellipse at all points below the surface of the membrane:

$$\frac{x_1^2}{Rc1^2} + \frac{x_2^2}{Rc2^2} = 1, \qquad x_3 \leqslant 0, \tag{19}$$

In other words, we have an infinitely long pore with its opening lying in the $x_3 = 0$ plane and the droplet is forming above this plane (see Fig. 6a). The energy contribution from the droplet's contact at the pore mouth is described below.

The energy arising from interfacial tension on the free surface (oil–surfactant solution interface) is a scalar function of the area and is an easily measured quantity. However, the contact between the oil and the membrane gives both energy and constrains the shape of the droplet. At this point is it important to remember the definition of contact angle, θ_c, which is not the physical angle at which the droplet's surface contacts the pore mouth, but a macroscopic measured quantity. The contact angle describes the relative size of the membrane–oil (MO) and membrane–aqueous (MA) phase interfacial tensions (i.e., energy densities J m^{-2}) with respect to the aqueous–oil (AO) phase interfacial tension:

$$\gamma_{\mathrm{MO}} + \gamma_{\mathrm{AO}} \cos\theta_c = \gamma_{MA} \text{ (Young equation)}, \tag{20}$$

$$\gamma_{\mathrm{AO}}(1 + \cos\theta_c) = \Delta G^*_{\mathrm{MO}} \text{ (Young–Dupré equation)}, \tag{21}$$

where ΔG^*_{MO} is the contact energy per unit area of the membrane surface and oil droplet surrounded by the aqueous phase. This contribution is modelled by giving the edge in contact with the surface an energy integrand [16]. Let **S** be the orientated droplet surface in contact with the membrane surface, T be the contact energy density and **i**, **j**, and **k** be the unit basis vectors. Then we want to find a vector field **W** such that

$$\int_{\substack{\text{contact}\\ \text{area}}} T\mathbf{k}\, d\mathbf{S} = \int_{\substack{\text{contact}\\ \text{line}}} \mathbf{W}\, d\mathbf{l}. \tag{22}$$

$T = (-\cos(\theta_c \times \pi/180))$ and θ_c is the interior angle between plane and surface [16].

Now by using Stokes' theorem [31]:

$$\operatorname{curl} \mathbf{W} = T\mathbf{k} \tag{23}$$

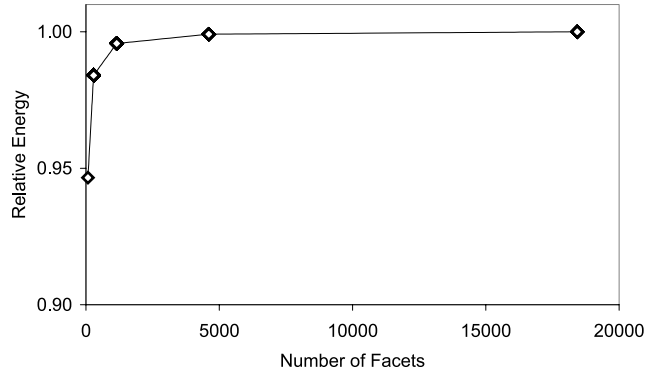

Fig. 7. Relative change in the surface energy as a function of number of calculation facets using the conditions of MC2-SURF1.

and thus we can use

$$\mathbf{W} = -Tx_2\mathbf{i}. \tag{24}$$

This gives the contact energy in the form of a line integral around the contact line which is constrained by the pore at $x_3 \leqslant 0$.

The input parameters of the model, which are adjustable at run-time, are pore geometry, initial volume of the droplet (equal to 40% of a ellipsoidal hemisphere, given by $2/3\pi Rc1 \times Rc2^2$) the oil–surfactant solution interfacial tension, and contact angle. The outputs of the Surface Evolver are images of the surface as it evolves (Figs. 6b and 6c), the total energy, surface area and volume of the droplet, and eigenvalue information for determining droplet stability.

The required level of refinement for the model (the number of triangles covering the surface) was found by considering a stable droplet and finding at which point the energy of the surface becomes independent of the refinement level. Fig. 7 shows such an exercise and plots the relative energy versus number of facets. As the number of facets increases, the deviation from unity decreases, and more accurate is the calculation. However, the number of facets exponentially increases the required computing resources, so a compromise is used. In this case the appropriate number of facets was found to be around 4000.

Table 1
Experimental values from [14] used to verify model

Name	$Rc1$ (μm)	$Rc2$ (μm)	R_h (μm)	γ (mN m^{-1})	θ_c (deg)	Diam.[e] (μm)
MC1-SURF1	26.3	7.00	22.1	4.4[a]	143	49.0 ± 1.4%
MC1-SURF2	26.3	7.00	22.1	1.9[b]	142	48.9 ± 2.1%
MC1-SURF3	26.3	7.00	22.1	23.4[c]	130	50.3 ± 1.9%
MC1-SURF4	26.3	7.00	22.1	1.4[d]	145	53.2 ± 3.3%
MC2-SURF1	24.4	4.80	16.0	4.4	143	38.9 ± 2.3%
MC2-SURF2	24.4	4.80	16.0	1.9	142	38.1 ± 1.9%

Emulsifiers:
[a] 1 wt% PGFE (pentaglycerol monolaurate);
[b] 1 wt% Tween 20 (polyoxyethylene 20 sorbitan monolaurate);
[c] No surfactant;
[d] 1 wt% SE (sucrose monoesterate).
[e] ± Coefficient of variation as %.

4.6. Validation of the model

Experimental results from Kobayashi and Nakajima [14] were used to validate the model. Their setup employed a straight-through microchannel which could be seen as an idealized membrane since there is no terrace or constricting glass plate to affect droplet formation. The uniform oblong shaped pores were microfabricated on a silicon substrate using deep reactive ion etching [13]. In addition to defined geometry, they also give data on the interfacial tension and contact angles for the systems they studied (see Table 1) which were used as input parameters for the Surface Evolver model.

The calculations were carried out as follows: The literature data were used to set up the initial surface in the program data file, the surface evolver program runs the program file and the user creates and initializes an output file to which the results from each calculation step are written. The surface is evolved by first doing a series of refinements (increasing the number of facets to improve accuracy) then increasing the droplet volume in small increment steps by adding 0.5% of the current volume. After each volume addition, a gradient descent is performed to obtain the surface configuration of lowest energy for that particular volume and given set of constraints; the surface area, volume, and total energy are calculated, as well as the Hessian's eigenvalues to determine if the droplet is approaching instability. The results from this step are written to the output file and the next volume addition occurs. This process iterates until the droplet becomes unstable (negative eigenvalues) the volume, surface area, and energy at which this occurs is noted. The final size of the detaching droplet then calculated using the pressure pinch constraint.

5. Results and discussion

Six sets of experimental conditions (Table 1) were simulated using the Surface Evolver. The results are shown in Fig. 8. The error bars on the mean experimental values represent the coefficient of variation given as a percent. The

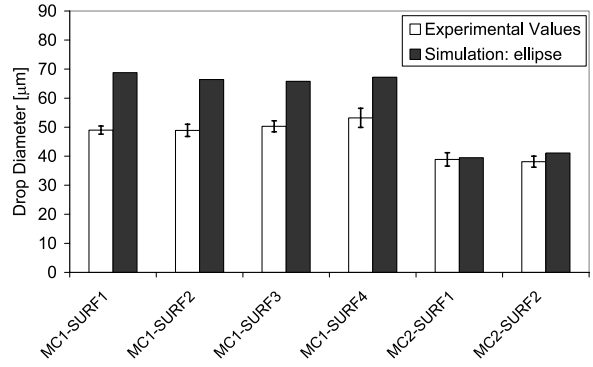

Fig. 8. Simulation results as compared to experimental data from Table 1. Error bars on experimental results (white) are CV%. Surface Evolver simulation results (black).

average error of the six simulations compared to experimental values was 18% and was larger for MC1 which had the larger of the two pore sizes. It was thought that the larger error on the first four simulations on MC1 could be due to the larger size of the pore opening (see Table 1) since droplet formation based only on the interfacial tension best describes small systems where the forces arising from flow are insignificant. This was also supported by the fact that the simulation over predicts the droplet size, meaning that the real droplet experiences an earlier instability. However, upon further analysis of the energies in the system it was seen that the energy arising from the contact tension at the pore played a significant role. This led to the realization that a proper representation of the pore geometry is tantamount to a good modelling result.

In the simulations results shown in Fig. 8, the pore was estimated to be an ellipse with a major and minor axis equal to the half-length and half-width of the pore opening given in the literature. This simplification was chosen since it was thought that the radii of curvature determined by length and width of the pore would essentially govern the maximum stable droplet volume for a given interfacial tension and contact angle. Upon close inspection of the micrographs of the pore openings used by Kobayashi and Nakajima [13–15] it was observed that the pores are in fact considerably rectangular in shape. This means that their perimeters are larger than an ellipse with the same length and width, and thus would also have greater pore energy, E_{pore}.

With this new insight, the model was improved to use a rectangular shaped pore. Since continuous functions are much easier to implement in the simulation, a superellipse was chosen (Fig. 9a) to represent a rectangle. The higher the value of rq the more rectangular the superellipse becomes. Using this new geometry (using rq equal to 100) the simulations were repeated and the results are compared to the experimental values (Fig. 10). There was a significant improvement in the simulation's results. The average error over the six simulations compared to experimental values was decreased to 8%. The exact geometry of the pores used by Kobayashi and Nakajima [14] is hard to know from the

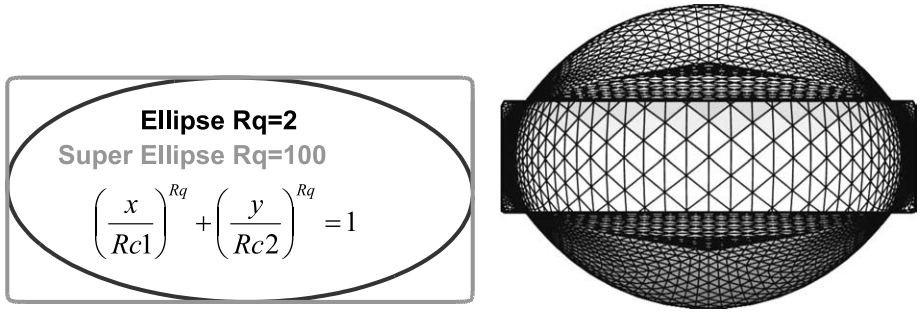

(a) (b)

Fig. 9. (a) Improved geometry using a superellipse, plot of ellipse and superellipse geometry. (b) Bottom view of a simulation.

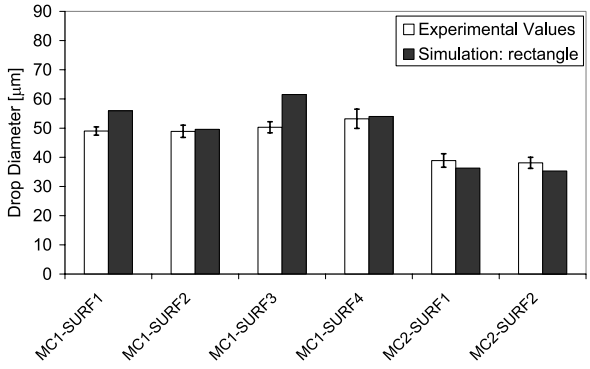

Fig. 10. Simulation results compared to data from Table 1 with superelliptical pore geometry. Error bars on experimental results (white) are CV%. Surface Evolver simulation results (black).

micrographs, but they do report the hydraulic radius, R_h, of their pores which is defined as 4 times the area divided by the perimeter. The hydraulic radius given for MC1 is 22.1 and 16.0 µm for MC2. The geometric details of the elliptical (indicated by the suffix E) and rectangular-superelliptical simulations (indicated by the suffix R) are given in Table 2. For the simulations using elliptical geometry, the R_h was under estimated by between 8% and 10% but R_h using rectangular-superelliptical geometries deviated by less than 0.8% from the literature data. This is an interesting result since the decrease in error of the hydraulic radius by switching from an ellipse to a rectangular superellipse is on the order of 10% and the decrease in the average error of the simulation also decreases by approximately 10%. This again underlines the importance of pore geometry in determining the quality of the model's results.

There was some concern that the model inadvertently prevented spreading of the oil across the surface of the membrane for the reason that after observing the images generated by the Surface Evolver it was seen that the 3-phase contact line did not expand beyond the edge of the pore. This could be a result of a mathematical effect of the definition of the boundary conditions used to calculate to contact energy at the pore or alternatively that spreading did not occur due to energetic grounds. To determine if the drop should spread, simulations were repeated by placing a droplet with a volume equal to the MSV of the case MC2-SURF1-R on a plane without a pore. The droplet was allowed to spread and obtain its lowest energy shape without the influence of a pore. However, inside the area representing a pore there is no energy penalty for wetting (see Eq. (21)) since it is an ellipsoid of oil contacted by the oil droplet. Therefore the total energy found for the spread drop case by the Surface Evolver should have this amount subtracted from it. The results of this investigation are found in Table 3.

In Table 3 the total energies of six configurations are calculated by the Surface Evolver. At the maximum stable volume (MSV) the total energy of an attached droplet is only slightly larger (0.24%) than a detached drop and plus the pore energy. If we increase the droplet's volume to 5% beyond the MSV it becomes unstable and its energy increases by 2 orders of magnitude while the energy detached droplet plus the pore at MSV + 5% remains almost unchanged. This exercise showed that the droplet plus the pore is energetically favorable at volumes exceeding the MSV. The last two columns in Table 3 consider the relative energies with respect to spreading. The total energy of a spread droplet with a volume equal to the MSV is 22 times larger than that the unspread droplet attached at the pore. Even if we subtract the above mentioned oil–oil energy penalty-free area the total energy of the spread drop minus the pore area is still more than 11 time larger than the unspread droplet. The energy of spreading the droplet is larger than the unspread pinned droplet; this suggests that spreading is not likely to happen for energetic reasons.

This nonspreading condition is essential in spontaneous transformation based droplet formation seen in membrane emulsification when the droplet to pore size ratio is approximately 3 and the droplet formation is almost monodispersed [3,4,9,12–15,32]. This nonspreading at the membrane pore mouth has been attributed to effects of a small dynamic contact angle by Christov et al. [32]. But in this modeling work there is no change of the interfacial tension with time. Another explanation of why the drops are pinned could be the line tension around the perimeter of the pore mouth, which, although in most cases small compared to the total energy of the system, can be important in resisting the local progress of the contact line [33].

The line tension can be defined as the reversible work per unit length which is necessary to expand isothermally

Table 2
Simulation results

Name	$Rc1$ (μm)	$Rc2$ (μm)	$Rc1/Rc2$	Area (μm^2)	R_h (μm)	γ (mN m^{-1})	θ_c (deg)	MSV (m^3)	V_{drop} (m^3)	V_{drop}/MSV	E_{pore} (J)	E_{surf} (J)	E_{tot} (J)
MC1-SURF1-E	26.3	7.00	3.8	577	20.4	4.4	143	6.94×10^{-13}	1.71×10^{-13}	0.246	4.61×10^{-10}	1.65×10^{-10}	6.26×10^{-10}
MC1-SURF1-R	26.3	7.00	3.8	732	22.2	4.4	143	3.68×10^{-13}	9.15×10^{-14}	0.249	5.84×10^{-10}	1.07×10^{-10}	6.93×10^{-10}
MC1-SURF2-E	26.3	7.00	3.8	577	20.4	1.9	142	6.20×10^{-13}	1.53×10^{-13}	0.248	4.54×10^{-10}	6.61×10^{-11}	5.20×10^{-10}
MC1-SURF2-R	26.3	7.00	3.8	732	22.2	1.9	142	2.27×10^{-13}	6.38×10^{-14}	0.281	5.79×10^{-10}	3.31×10^{-11}	6.12×10^{-10}
MC1-SURF3-E	26.3	7.00	3.8	577	20.4	23.4	130	6.00×10^{-13}	1.49×10^{-13}	0.248	3.71×10^{-10}	7.96×10^{-10}	1.17×10^{-9}
MC1-SURF3-R	26.3	7.00	3.8	732	22.2	23.4	130	4.71×10^{-13}	1.22×10^{-13}	0.259	4.72×10^{-10}	6.73×10^{-10}	1.15×10^{-9}
MC1-SURF4-E	26.3	7.00	3.8	577	20.4	1.4	145	6.30×10^{-13}	1.59×10^{-13}	0.253	4.74×10^{-10}	4.92×10^{-11}	5.23×10^{-10}
MC1-SURF4-R	26.3	7.00	3.8	732	22.2	1.4	145	3.04×10^{-13}	8.24×10^{-14}	0.271	6.02×10^{-10}	2.98×10^{-11}	6.32×10^{-10}
MC2-SURF1-E	24.4	4.80	5.1	367	14.4	4.4	143	1.22×10^{-13}	3.23×10^{-14}	0.265	2.93×10^{-10}	5.12×10^{-11}	3.44×10^{-10}
MC2-SURF1-R	24.4	4.80	5.1	467	16.1	4.4	143	8.67×10^{-14}	2.50×10^{-14}	0.288	3.73×10^{-10}	4.04×10^{-11}	4.14×10^{-10}
MC2-SURF2-E	24.4	4.80	5.1	367	14.4	1.9	142	1.38×10^{-13}	3.62×10^{-14}	0.262	2.89×10^{-10}	2.41×10^{-11}	3.13×10^{-10}
MC2-SURF2-R	24.4	4.80	5.1	467	16.1	1.9	142	7.86×10^{-14}	2.30×10^{-14}	0.292	3.68×10^{-10}	1.63×10^{-11}	3.84×10^{-10}
MC2-SURF1-RθA	24.4	4.80	5.1	467	16.1	4.4	140	9.70×10^{-14}	2.75×10^{-14}	0.284	3.58×10^{-10}	4.36×10^{-11}	4.01×10^{-10}
MC2-SURF1-RθB	24.4	4.80	5.1	467	16.1	4.4	143	1.02×10^{-13}	2.87×10^{-14}	0.282	3.73×10^{-10}	4.51×10^{-11}	4.18×10^{-10}
MC2-SURF1-RθC	24.4	4.80	5.1	467	16.1	4.4	146	9.10×10^{-14}	2.61×10^{-14}	0.286	3.87×10^{-10}	4.17×10^{-11}	4.29×10^{-10}

MSV: maximum stable volume of an attached droplet, R_h: hydraulic diameter $R_h = 4 \times$ area/perimeter.

the length of the 3-phase contact line, or in other words the difference between the actual energy of the system and the sum of the energies of the individual ideal interfaces [34]. This correction to the free energy due to the line tension is usually calculated by considering the modification of the droplet profile close to the contact line due to van der Waals forces [35]. However, this theoretical modification from van der Waals forces is on the order of 10^{-12} N and only fits well for liquid systems. When solids are involved, for example, liquid droplets on solid substrates, the line tension effect is much bigger than what is predicted by van der Waals forces alone, reported in the range 10^{-11}–10^{-5} [36]. This difference is thought be caused by the surfaces not being ideally flat and smooth. It has been shown that curved surfaces can have a significant effect on the line tension result [34,36] and thermodynamic studies predict that a positive line tension can induce a stability crisis in the equilibrium of a 3-phase system. A positive line tension has the effect of tightening the contact line and in the case of a small sessile droplet on a solid substrate, thus the line tension can induce a wetting/drying transition [36]. In Table 3 the line tension energy E_{LT} is calculated as the difference between the total energy found by the Surface Evolver and the sum of energy contributions of the individual interfaces (i.e., $E_{total} - E_{surf} - E_{pore}$) for the case of the droplet at MSV with the geometric constraint of the pore. Here we find a small positive E_{LT} which then becomes a large negative E_{LT} as the droplets volume is increased beyond its maximum stable volume. Experimental values of line tensions for droplets on this size scale are not easily obtained, nor are the exact geometry and surface smoothness of the real solid surface; however, line tension effects may explain why these droplets can spontaneously detach, as well as why slot shaped pores and ceramic membranes with large pore perimeter to pore area ratios perform better in membrane emulsification applications.

The model's sensitivity to the two parameters which are not geometric in nature was also considered. In Fig. 8 the first condition (MC1-SURF1) has an interfacial tension which is almost twice the second condition (MC1-SURF2) but their contact angles only differ by 1°. Despite the difference in interfacial tension, the results are almost identical. To determine the effect of contact angle on the simulation result, three additional conditions were simulated (Table 2: MC2-SURF1-RθA, B and C) where the contact angle was changed in 3° increments. This caused E_{total} to increase by 4% between 140° and 143°, and increase by 2.5% between 143° and 146°. The increase in total energy directly corresponds to the increase in the value of the contact energy density ($T = -\cos(\theta \times \pi/180)$). The change in the predicted droplet diameter due to a small change in contact angle is not as well-defined as the energy increase but remains on the order of 3–4%. This means that a good estimation of the contact angle is also imperative.

Table 3
Comparison of energy to justify the nonspreading condition of the oil phase

	MC2-SURF1-R		Detached drop + pore		Spread drop at MSV	
	MSV	MSV + 5%	MSV	MSV + 5%	Contact	Minus pore area
Geometry						
Droplet volume (m^3)	8.67E−14	9.10E−14	8.67E−14	9.10E−14	8.67E−14	8.67E−14
Pore area (m^2)	4.67E−10	4.67E−10	4.67E−10	4.67E−10	–	4.67E−10
3 Phase perimeter (m)	1.12E−04	1.12E−04	1.12E−04	1.12E−04	1.05E−04	1.05E−04
Spread contact area (m^2)	–	–	–	–	8.84E−10	4.17E−10
Oil–water Interfacial area (m^2)	9.17E−09	2.35E−05	9.47E−09	9.79E−09	8.71E−09	8.71E−09
Energy (J)						
E_{tot} from Surface Evolver	**4.14E−10**	**8.85E−08**	**4.15E−10**	**4.16E−10**	**9.14E−09**	**4.70E−09**
E_{surf} (o–w interface)	4.04E−11	1.03E−07	4.17E−11	4.31E−11	3.83E−11	3.83E−11
E_{pore}/contact (oil–memb.)	3.73E−10	3.73E−10	3.73E−10	3.73E−10	9.10E−09	4.67E−09
E_{LT}	8.62E−16	−1.53E−08	–	–	–	–

MSV: maximum stable volume of an attached droplet.

6. Summary

Using the finite element calculation environment of the Surface Evolver, a model was developed to describe spontaneous transformation based droplet formation from a well defined membrane. This model reasonably predicts the droplet size in quiescent conditions where the force balance approach is not applicable. Despite the fact that no empirical fitting parameters were employed, and that the model uses only geometric and physical properties of the system, the error of the predictions was on average only 8% using the rectangular-superelliptical geometry.

With this model and the Surface Evolver program it is possible to consider a myriad of combinations of pore geometries, interfacial tensions and contact angles. This allows one to study the largest stable volume that can be formed from a pore, and thus allow predictions of final droplet volumes which do not depend on a force balance approach or the necessity of a cross-flow. Predicting the maximum stable droplet volumes and knowing their relationship to pore geometry, will significantly aid in the design of membranes through optimizing pore size, shape, and spacing.

Acknowledgments

This project was financially supported by LiFT—Future Technologies for Food Production, a national, industry-oriented Swedish programme for research and Ph.D. education. Fruitful discussions with Dr. Jenny Olsson were greatly appreciated.

Appendix A. Notation

A Area (m^2)
Bo Bond number (–)
Ca Capillary number (–)
D Diameter (m)
E, E_{mech}, E_{surf}, E_{pore}, E_{LT} Energy, mechanical, surface, pore, line tension (J)
$E_{Laplace}$, E_{total} Energy associated to Laplace pressure, total energy from Surface Evolver (J)
$\widehat{E}(\mathbf{x})$, $\widehat{E}_0$, $\widehat{E}_{min}$ Energy function, original value, minimum of energy function (J)
F, F_γ, F_{sp}, F_L, F_B, F_I Force, interfacial, static pressure, lift, buoyancy, inertial (N)
f Helmholtz free energy (J)
G, ΔG Gibbs free energy, change in free energy (J)
ΔG^* Young–Dupré contact energy per unit area ($J\,m^{-2}$)
$\mathbf{G}$ Gradient of energy function
H Enthalpy (J)
$\mathbf{i}$, $\mathbf{j}$, $\mathbf{k}$ Unit basis vectors
$d\mathbf{l}$ Oriented differential line element (m)
P, $P_{Laplace}$, P_{in}, P_{out} Pressure, Laplace pressure, pressure inside and out of droplet (Pa)
$P_{attached}$, P_{break} Pressure across attached surface, pressure of droplet that breaks off (Pa)
R, R_{break} Radius, radius of droplet that breaks off (m)
Re Reynolds number (–)
R_h Hydraulic radius (m, μm)
rq Superelliptical exponent (–)
S Entropy ($J\,K^{-1}$)
$d\mathbf{S}$ Oriented differential surface element (m^2)
T Temperature (K)
U Velocity ($m\,s^{-1}$)
V, V_{break}, V_{final}, $V_{attached}$ Volume, breaking droplet (m^3)
W Work (J)
$\mathbf{W}$ Vector field for calculating contact energy density along $d\mathbf{l}$
We Weber number (–)
x_1, x_2, x_3 Cartesian position coordinates in the $\mathbf{i}$, $\mathbf{j}$, and $\mathbf{k}$ directions
γ Interfacial tension ($N\,m^{-1}$)
γ_{MO}, γ_{MA}, γ_{AO} Membrane–oil (MO), membrane–aqueous (MA) aqueous–oil (AO) ($N\,m^{-1}$)
μ Viscosity (Pa s)
θc Contact angle (°)

ρ, $\Delta\rho$ Density, density difference between phases ($kg\,m^{-3}$)
T Contact energy density ($J\,m^{-1}$)
τ_w Wall shear stress (Pa)

References

[1] S.J. Peng, R.A. Williams, Trans. Inst. Chem. Eng. 76 (1998) 894.
[2] H. Schubert, in: Proceedings of Engineering and Food ICEF 7, 13–18 April, Brighton, UK, Academic Press, San Diego, 1997, p. AA82.
[3] S.M. Joscelyne, G. Trägårdh, J. Food Eng. 39 (1998) 59.
[4] K. Kandori, in: A.G. Ganokar (Ed.), Food Processing: Recent Developments, Elsevier, Amsterdam, 1995, p. 113.
[5] T. Kawakatsu, Y. Kikuchi, M. Nakajima, J. Am. Oil Chem. Soc. 74 (1997) 317.
[6] S. Sugiura, M. Nakajima, S. Iwamoto, M. Seki, Langmuir 17 (2001) 5562.
[7] T. Kawakatsu, H. Komori, M. Nakajima, Y. Kikuchi, T. Yonemoto, J. Chem. Eng. Jpn. 13 (1999) 241.
[8] T. Kawakatsu, G. Trägårdh, Y. Kikuchi, M. Nakajima, H. Komori, T. Yonemoto, J. Surfactants Deterg. 3 (2000) 295.
[9] V. Schröder, O. Behrend, H. Schubert, J. Colloid Interface Sci. 202 (1998) 334.
[10] Z. Wang, S. Wang, V. Schröder, H. Schubert, Chinese J. Chem. Eng. 8 (2000) 108.
[11] M. Rayner, G. Trägårdh, Desalination 145 (2002) 165.
[12] M. Yasuno, M. Nakajima, S. Iwamoto, T. Maruyama, S. Sugiura, I. Kobayashi, A. Shono, K. Satoh, J. Membrane Sci. 210 (2002) 29.
[13] I. Kobayashi, M. Nakajima, K. Chun, Y. Kikuchi, H. Kukita, AIChE J. 48 (2002) 1639.
[14] I. Kobayashi, M. Nakajima, Eur. J. Lipid Sci. Technol. 104 (2002) 720.
[15] I. Kobayashi, M. Nakajima, in: Proceedings: International Microprocess and Nanotechnology Conference, November 6–8, Tokyo, Japan, 2002, p. 274.
[16] K. Brakke, The Surface Evolver, www.susqu.edu/facstaff/b/brakke/evolver/html/default.htm, 1999.
[17] K. Brakke, Exp. Math. 2 (1992) 141.
[18] K. Brakke, Philos. Trans. R. Soc. A 354 (1715) (1996) 2143.
[19] K. Brakke, F. Morgan, Eur. Phys. J. E 9 (2002) 453.
[20] Q. Zhu, G. Wang, L. Lou, in: Solid-State and Integrated Circuit Technology IEEE Proceedings, 1998, p. 554.
[21] G. McHale, M.I. Newton, Colloids Surf. A 206 (2002) 79.
[22] J. Silver, Z. Mi, K. Takamoto, P. Bungay, J. Brown, A. Powell, J. Colloid Interface Sci. 219 (1999) 81.
[23] G. Bradley, D. Weaire, Comput. Sci. Eng. 6 (2001) 16.
[24] K. Brakke, Hessian, Eigenvalues, Eigenvectors and Stability in the Surface Evolver, www.susqu.edu/facstaff/b/brakke/evolver/html/eigentut.htm, 1999.
[25] H.R. Kemp, Phys. Educ. 19 (1984) 234.
[26] Y.H. Mori, AIChE J. 36 (1990) 1272.
[27] G.F. Scheele, B.J. Meister, AIChE J. 14 (1968) 9.
[28] R. Kumar, N.R. Kuloor, in: T.B. Drew, G.R. Cokelet, J.W. Hoopes, T. Vermeulen (Eds.), Advances in Chemical Engineering, Academic Press, New York, 1970, p. 8.
[29] A.H.P. Skelland, E.A. Slaymaker, Ind. Eng. Chem. Res. 29 (1990) 494.
[30] J. Pellicer, V. Garcia-Morales, M.J. Hernádez, Phys. Educ. 35 (2000) 126.
[31] G. Arfken, Mathematical Methods for Physicists, third ed., Academic Press, London, 1985.
[32] N.C. Christov, D.N. Ganchev, N.D. Vassileva, N.D. Denkov, K.D. Danov, P.A. Kralchevsky, Colloids Surf. A 209 (2002) 83.
[33] J.F. Oliver, C. Huh, S.G. Mason, J. Colloid Interface Sci.59 (1977) 568.
[34] A. Marmur, B. Krasovitski, Langmuir 18 (2002) 8919.
[35] A. Checco, P. Guenoun, J. Daillant, Phys. Rev. Lett. 91 (2003) 186101.
[36] J. Faraudo, F. Bresme, J. Chem. Phys. 118 (2003) 6518.